A SINGLE LASER OPERATED COLD ATOM GRAVIMETER

K. Bhardwaj [a], *S. Singh* [a], *S. P. Ram* [a*], *B. Jain* [a], *V. Kumar* [a,c], *A. Pathak* [b], *S. Tiwari* [b],

V. B. Tiwari [a,c], *S. R. Mishra* [a,c]

[a] *Laser Physics Applications Division, Raja Ramanna Centre for Advanced Technology*
452013, Indore, India

[b] *Laser Controls and Instrumentation Division, Raja Ramanna Centre for Advanced Technology*
452013, Indore, India

[c] *Homi Bhabha National Institute, Training School Complex, Anushakti Nagar*
400094, Mumbai, India

A cold atom gravimeter (CAG) using a single laser system has been developed. In the setup, the laser cooled ^{87}Rb atoms are launched in the vertical upward direction and Doppler sensitive two-photon Raman pulse atom interferometry is applied to measure the gravitational acceleration g experienced by the atoms. Using our gravimeter setup, we have measured the local value of g in our laboratory with a sensitivity of 621 μGal for integration time of 1350 s. The use of single laser system keeps our CAG setup simple and compact, and does not require the phase-locking of different lasers.

1. INTRODUCTION

For nearly three decades, research and developments in the field of cooling and trapping of neutral atoms have witnessed various applications of cold atoms in the study of fundamental science as well as in the development of advanced quantum technologies [1]. Using laser cooled atoms, various fundamental physics problems have been studied including Bose-Einstein condensation [2], degenerate Fermi gases [3], equivalence principle [4], measurement of fundamental constants [5,6], gravitational waves [7,8], etc. On the devices side, the laser-cooled atoms have shown their strong applications in developing state-of-art precision quantum sensors and metrology devices such as atomic clocks [9], atomic accelerometers or gravimeters [10–15], atom gyroscopes [16,17], atomic sensors of electromagnetic fields [18], magnetometers [19,20], etc. In the world-wide scenario, there is also considerable interest in the trapping and manipulation of the single atom for its use as a qubit for quantum information process-

ing [21]. Due to involvement of fundamental principles of quantum physics in the working of these devices, the cold atoms based quantum devices have shown inherent superiority as compared to existing advanced classical devices [22,23].

After the first proposal and demonstration by Kasevich and Chu in 1991 [24], cold atom interferometry has become a popular method for precision measurement of inertial parameters such as acceleration [25–32] and rotation [33]. A cold atom gravimeter (CAG) is an instrument developed using cold atoms for the precision measurement of the gravitational acceleration g of the Earth. This is an advanced quantum sensor which can measure the absolute value of gravitational acceleration with high precision. As compared to light interferometry based gravimeters, the CAG does not have any mechanical abrasion for the test mass used in the measurements, which helps in increasing the repetition rate of measurements and maintaining device without frequent calibrations. Due to variations in the density of mass in the body of the Earth, the value of gravitational acceleration g of the Earth varies from place to place on the Earth's surface. The value of g at a given place may also vary temporally during underground seismic activities. Both types of variation in the g-value are very

* E-mail: spram@rrcat.gov.in
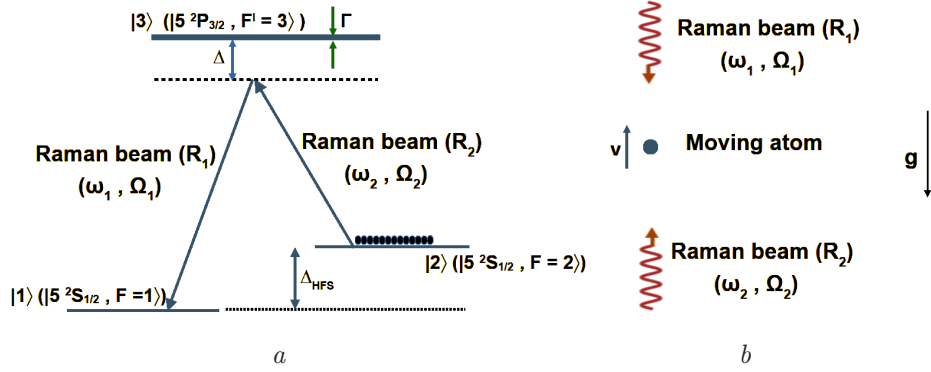
Fig. 1. *a* — *The schematic of the energy levels of* ^{87}*Rb atom involved in two-photon Raman transition in the atom interferometer. Here* Δ *is detuning of Raman beams from the level* $|3\rangle$ *and* Δ_{HFS} *is the hyperfine splitting between two states* $|1\rangle$ *and* $|2\rangle$. *b* — *Schematic of geometry of the counter-propagating Raman beams interacting with a moving atom*

small, requiring a high-sensitivity gravimeter to measure them. A gravimeter with such high sensitivity has applications in underground mineral explorations [34], monitoring seismic activities [35], detection of underground tunnels and structures, geophysics study [36], etc. Accurate gravimeters also find applications in inertial navigation and in space missions for microgravity experiments [37, 38]. A cold atom gravimeter is an absolute gravimeter with high sensitivity, accuracy, and long-term stability [25, 39]. The high accuracy of a CAG originates from the quantum nature of atom-light interaction, in which a two-photon Raman transition in an atom is probed with high accuracy.

Here we present the development of a cold atom gravimeter (CAG) setup employing a single laser system. This gravimeter is based on the well-known method of Doppler-sensitive two-photon Raman pulse atom interferometry involving two hyperfine levels in the ground state of ^{87}Rb atom. The atom interferometry is performed when laser cooled ^{87}Rb atoms are launched in the vertical upward direction as done in an atomic fountain [28, 40]. The cold atoms are prepared in a magneto-optical trap (MOT) setup similar to that reported earlier [41]. Various laser beams used in this gravimeter are derived from the output of a single laser system. The use of single laser system keeps the CAG setup compact and does not require the complicated phase locking procedure between different laser beams used in the Raman pulse atom interferometry. Using this CAG set-up, we have estimated the local value of g in the laboratory to be $9.786173 \, \mathrm{m/s^2}$ at the resolution of $270 \, \mu$Gal ($\sim 0.000003 \, \mathrm{m/s^2}$). estimated from the frequency chirp rate applied to a Raman beam to achieve a maximum in the interferometric fringes. We have assessed the performance of the gravimeter by measuring the Allan deviation in g-measurements. The observed

minimum value of the Allan deviation was $\sim 621 \, \mu$Gal for an integration time of 1350 s. Though the precision of our gravimeter is slightly inferior as compared to the recent atom gravimeters reported, our CAG system is relatively simple and compact because of use of single laser system.

2. WORKING PRINCIPLE OF COLD ATOM GRAVIMETER

The cold atom gravimeter (CAG) discussed here is based on the velocity-sensitive two-photon Raman excitation which has been described in several research works [28, 29, 42, 43]. For the measurement of g, the cold atoms in our CAG are launched against the gravitational acceleration g, and a velocity sensitive two-photon Raman transition between two hyperfine states is monitored. The Raman transition is driven by interferometric $\pi/2$-T-π-T-$\pi/2$ pulses of two counterpropagating Raman beams, where T is the duration of free evolution between the pulses of Raman beams [24]. Fig. 1 shows the schematic of such a Raman transition in an atom between states $|1\rangle$ and $|2\rangle$ via an intermediate state $|3\rangle$. Since the velocity of an atom continues to change due to gravitational acceleration (g), the Raman transition probability after the sequence of Raman pulses becomes dependent on the value of g and duration T. Thus, this modified transition probability can provide the value of g acting on the atom.

Figure 1 a shows the energy levels of ^{87}Rb atom involved in two-photon Raman transition in the atom interferometer. The Raman beams R_1 and R_2 at frequencies ω_1 and ω_2, with coupling strengths Ω_1 and Ω_2, are kept in counter-propagating arrangement as shown in Fig. 1 b. When an atom is moving with speed v against the direction of gravitational acceleration and

in the direction of the Raman beam R_2 (Fig. 1 b), the two-photon Raman resonance condition is given as

$$\omega_1 = \omega_2 + \Delta_{HFS} - (k_1 + k_2)v,$$

with $k_i(i = 1, 2)$ are wave-vector magnitudes for two Raman beams.

When the detuning (Δ) is kept large to avoid a single-photon transition, this three-level system can be approximated to a two-level system with effective Rabi frequency for coupling of levels $|1\rangle$ and $|2\rangle$ as

$$\Omega_{eff} = \Omega_1\Omega_2/2\Delta.$$

If one considers multiple excited states instead of a single intermediate state $|3\rangle$, then the effective Rabi frequency (Ω_{eff}) for Raman transition between $|1\rangle$ and $|2\rangle$ is calculated by summing over all allowed intermediate excited levels (i) as [44],

$$\Omega_{eff} = \sum_i \frac{\Omega_{1i}^*\Omega_{i2}}{2\Delta_i}, \tag{1}$$

where the index i for summation runs over all the possible intermediate excited states, Δ_i is detuning of the Raman beams from the state $|i\rangle$, and Ω_{1i} and Ω_{2i} are respectively the single photon Rabi coupling strengths of Raman beams for the transitions from states $|1\rangle$ and $|2\rangle$ to state $|i\rangle$.

If an atom is prepared in the initial state $|2\rangle$, its probability to remain in the level $|2\rangle$, after interacting with Raman beams for a time duration of t, is given as [43]

$$|C_2(t)|^2 =$$
$$= \left\{\cos^2\left(\frac{\Omega_R t}{2}\right) + \left(\frac{\delta - \delta_{AC}}{\Omega_R}\right)^2 \sin^2\left(\frac{\Omega_R t}{2}\right)\right\}. \tag{2}$$

Here the net coupling strength Ω_R is defined as

$$\Omega_R = \sqrt{\Omega_{eff}^2 + (\delta - \delta_{AC})^2},$$

with

$$\delta_{AC} = \Omega_1^{AC} - \Omega_2^{AC}$$

as difference of AC-Stark shifts in levels $|1\rangle$ and $|2\rangle$, and δ as two-photon detuning of Raman beams from resonance condition given by

$$\delta = (\omega_1 - \omega_2) - \Delta_{HFS} + (k_1 + k_2)v.$$

The population in level $|2\rangle$ (proportional to $|C_2(t)|^2$) shows Rabi oscillations with variation in time duration «t» of Raman beams. These oscillations strongly depend on the intensity of the Raman beams, detuning

Δ from the excited state (level $|3\rangle$), and two-photon Raman detuning δ. The measurement of these Rabi oscillations are used to estimate the duration of π-pulse for Raman pulse atom interferometry.

For the measurement of g by Raman pulse atom interferometry method, a sequence of $\pi/2 - T - \pi - T - \pi/2$ pulses of counter propagating Raman beams is applied on the atom cloud when the cloud is moving under the influence of gravitational acceleration. These Raman beams pulses create a Mach–Zehnder type interferometer for the moving atomic wave-packet [25, 39]. The separation T between the Raman pulses in the interferometer (in ms) is kept much larger than the duration of each Raman pulse (in μs). After interaction with the Raman beams pulses, the populations in levels $|1\rangle$ and $|2\rangle$ get modified. If there are N number of ^{87}Rb atoms prepared initially in the hyperfine state $|F = 2\rangle$ (i. e., level $|2\rangle$), the modified populations in two hyperfine states $|F = 2\rangle$ and $|F = 1\rangle$ after the Raman pulses ($\pi/2 - T - \pi - T - \pi/2$), are given as

$$N_{|F=2\rangle} = \frac{N}{2}[1 + \cos(\Delta\Phi)], \tag{3}$$

and

$$N_{|F=1\rangle} = \frac{N}{2}[1 - \cos(\Delta\Phi)], \tag{4}$$

where $\Delta\Phi = k_{eff}gT^2$ is the phase accumulated in the atom interferometer due to motion of atoms in the gravitational field. The parameter $k_{eff} = (k_1 + k_2) \approx 2k_1$ is the effective wave-vector magnitude of two counter propagating Raman beams, and k_1 is the wave-vector magnitude of a single Raman beam [25, 39]. Thus, by measuring the populations in the hyperfine states $|F = 1\rangle$ and $|F = 2\rangle$, after the Raman pulses, the phase $\Delta\Phi$ can be known. From the value of $\Delta\Phi$, g can be estimated for a given T.

For the estimation of g by this atom interferometry, it is convenient to introduce the chirp in the frequency of one of the Raman beams during the Raman pulses applied in the atom interferometer. With one Raman beam having a frequency chirp, the interacting atom experiences the time varying frequency difference between two Raman beams in the interferometer, which makes the interferometer phase to be dependent on the chirp rate. If α is the frequency chirp rate applied to one Raman beam, the net phase in the interferometer after the Raman pulses becomes

$$\Delta\Phi = k_{eff}gT^2 - 2\pi\alpha T^2.$$

As a result of this, the population in the either ground hyperfine state in the interferometer output oscillates
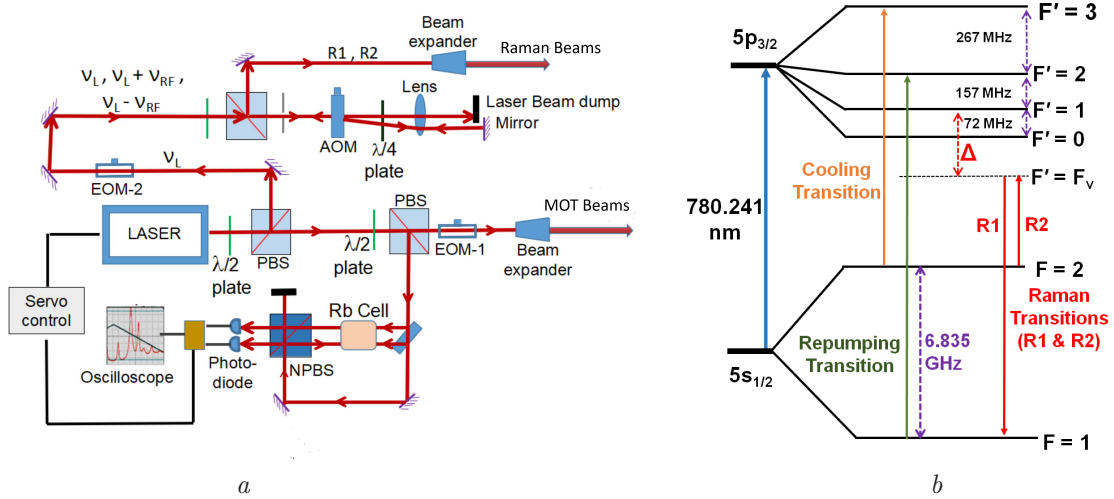
Fig. 2. *a* — *Schematic of the optical layout for generation of Raman beams and MOT beams used in the cold atom gravimeter (CAG). b — The schematic of energy levels of* ^{87}*Rb involved in cooling, repumping and Raman transitions in the CAG setup*

with the variation in the chirp rate (α). These oscillations in the population in the interferometer output are referred as interference fringes. The oscillation period in the fringes, a measure of the sharpness of the fringes, is dependent on the value of T. For a larger value of T, the fringes have a smaller period of oscillations with increased sharpness. Thus a larger value of T can improve the measurement resolution.

In the atom interferometer output, if the population is measured in the initial state $|F = 2\rangle$ (in our case) as function of α, then peaks in the observed interference fringes correspond to zero (or multiple of 2π) value of the net phase in the interferometer. The fringes observed for different values of T have a common maximum at a particular value of the chirp rate ($\alpha = \alpha_c$). At this chirp rate, called central chirp rate (α_c), the net phase in the interferometer is zero. Thus, by measuring the value of α_c, one can measure the value of g as,

$$\Delta\Phi = k_{eff}gT^2 - 2\pi\alpha_c T^2 = 0,$$

or

$$g = 2\pi\alpha_c/k_{eff} = \alpha_c\lambda/2, \qquad (5)$$

where $\lambda = 2\pi/k_1$ is the wavelength of the Raman beam.

3. EXPERIMENTAL SETUP

The CAG setup consists of a magnet-optical trap (MOT) for ^{87}Rb atoms for preparation of cold atoms. The laser cooled atoms are launched in vertical upward direction for performing Raman pulse atom interferometry and measuring the value of g. In this setup, all the laser beams needed from MOT formation to Raman

pulse atom interferometry, are derived from the output of a single laser system (DLC-TA-Pro, TOPTICA, Munich, Germany) operating at 780 nm wavelength. The use of single laser system makes our gravimeter system compact and easy to use [41]. Figure 2 *a* shows the schematic of optical layout for generation of MOT beams and Raman beams and Fig. 2 *b* shows the relevant transitions in ^{87}Rb atom used in cooling, repumping, and Raman pulse atom interferometer.

The output beam from the laser system (DSLC-TA-Pro) is divided into two parts. The first part is used to generate the MOT beams and the beams for frequency locking using saturated absorption spectroscopy (SAS) in a Rb-cell. The laser beam for MOT is passed through an electro-optic phase modulator EOM-1 (as shown in Fig. 2 *a*) operating at 6.58 GHz to generate laser emissions near to cooling and repumping transitions of ^{87}Rb atom (Fig. 2 *b*). The output laser beam from EOM-1 is split into two beams which are passed through two independent acousto-optic modulators (AOMs) to have fine control of frequency and power in the beams. The output of each AOM is then split into three beams, to obtain six MOT beams. Further, three MOT beams controlled by the one AOM are directed to the UHV chamber from the lower side viewports so that they are propagating in upward direction (as shown in Fig. 3). The remaining three MOT beams, controlled by the other AOM, are directed to UHV chamber from the upper side viewports on the chamber so that they are propagating in downward direction (as shown in Fig. 3). The power in each of six MOT beams is kept ~ 15 mW with $1/e^2$ beam radius as ~ 6 mm. All six MOT beams intersect one another at the centre of the UHV cham-
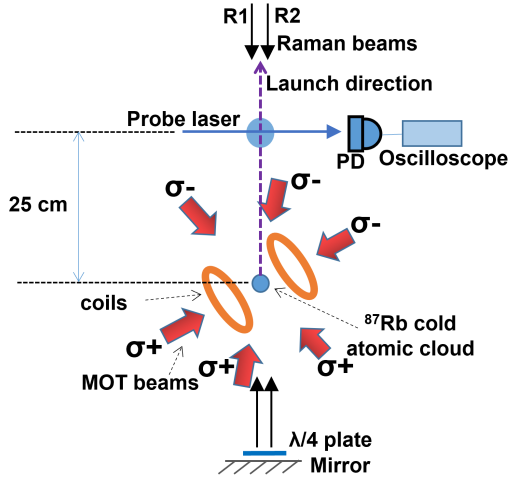
Fig. 3. Schematic of the atomic fountain based cold atom gravimeter setup

ber where zero of the quadrupole magnetic field is set. From MOT, the cold atoms are launched in the vertical direction by changing the detuning of the downward propagating MOT beams.

The second part of the laser beam from DLC-TA-Pro is passed through a second electro-optic modulator EOM-2 (as shown in Fig. 2 a) to generate Raman beams. When the laser beam at frequency ν_L is passed through the EOM-2 working at $\nu_{RF} \sim 6.83$ GHz, output beam contains the emission at three frequencies ν_L, $\nu_L + \nu_{RF}$ and $\nu_L - \nu_{RF}$ having powers in a ratio of $3 : 1 : 1$. The output beam from EOM-2 is double-passed through an acousto-optic modulator (AOM) working at 350 MHz, which results in a downshift to the emission frequencies by 700 MHz. The AOM output emissions at frequencies $\nu_1 = \nu_L + \nu_{RF}$ — 700 MHz and $\nu_2 = \nu_L$ — 700 MHz serve as Raman beams R_1 and R_2 with angular frequencies as $\omega_1 = 2\pi\nu_1$ and $\omega_2 = 2\pi\nu_2$. When laser system frequency is locked near the C_{13} cross-over peak in $|F = 2\rangle$ hyperfine transitions in ^{87}Rb atom, the Raman beam R_2 is red detuned by $\Delta \sim 476$ MHz from

$$|5^2 S_{1/2} F = 2\rangle \rightarrow |5^2 P_{3/2} F' = 1\rangle$$

transition. The total power in both the Raman beams R_1 and R_2 was ∼16 mW with a beam size (diameter) of ∼ 12 mm. The frequency chirp in the Raman beam is implemented by varying the frequency of RF source (ν_{RF}) in the EOM-2 through an arbitrary wave function generator (Tektronix–AFG3102C). Both the Raman beams enter into the chamber from the top and are retro-reflected from a mirror kept below the chamber. The polarization of the reflected beams are rotated

by 90 degree by keeping a quarter-wave plate before the retro-reflecting mirror as shown in Fig. 3.

We implement the (1,1,1) configuration for MOT beams. In this configuration, the vertical direction is (1,1,1) direction with coordinates axes being in the direction of the MOT beams (Fig. 3). In this configuration, the MOT beams do not hinder the path of atoms when they are launched in the vertical direction for atom interferometry measurements of g. A pair of coils is used to generate the quadrupole magnetic field with axial gradient of ~ 10 G/cm for MOT. The Rb vapor is injected into the chamber by passing a DC current in the Rb-dispenser source (SAES Rb getter). The MOT of ^{87}Rb atoms is loaded from the background vapor and the atom cloud at a temperature of ~ 25 μK with $1.8 \cdot 10^7$ number of atoms is obtained after the molasses stage.

For launching of atoms in vertically upward direction, the frequency of three MOT beams propagating in downward direction from upper side of the chamber is shifted to red with respect to the frequency of the other three MOT beams [41]. The launch velocity of atoms is dependent on this frequency shift [28]. For the detection of launched atoms (number and state), a horizontal probe laser beam at a particular height ($\sim$ 25 cm from the MOT centre) is aligned as shown in Fig. 3. The resonant absorption of this probe beam by the atoms crossing the probe beam gives the information of number of atoms and their state. We have used a probe beam of 1 mm size ($1/e^2$ radius) and ~ 5 μW power. It is observed that number of atoms reaching at the probe beam is dependent on the initial temperature of the atom cloud before launch.

Laser cooled ^{87}Rb atoms prepared in $|F = 2\rangle$ hyperfine state are launched to perform atom inteferometry. The stray magnetic field (~ 500 mG) removes the degeneracy of the hyperfine levels $|F = 2\rangle$ and $|F = 1\rangle$ which get connected by Raman beams. The Raman beams excite the transition

$$|F = 2, m_F = 0\rangle \rightarrow |F = 1, m_F = 0\rangle$$

due to $\pi^+ - \pi^-$ selection rules [45]. In order to ascertain that no other Zeeman sublevel in $|F = 1\rangle$ gets populated during this Raman excitation, we have probed absorption from Zeeman sublevels $|F = 1, m_F = +1\rangle$ and $|F = 1, m_F = -1\rangle$ after applying a π-pulse of Raman beams on the atom cloud (in $|F = 2\rangle$ state). The Raman beams pulse was applied after ~ 5 ms of launch, and the absorption signal of a probe beam at 9 cm height was recorded. The frequency of this probe was tuned to $|F = 1\rangle \rightarrow |F' = 0\rangle$ transition. It was observed that probe absorption was significant only when

probe beam polarization was linear and corresponding to π-polarization for the transition

$$|F = 1, m_F = 0\rangle \rightarrow |F^{'} = 0, m_{F'} = 0\rangle.$$

There was negligible absorption of probe, when probe beam polarization was made circular polarization (left handed and right handed). A fine tuning of frequency of circularly polarized probe beam also did not significantly change the probe absorption. These observations indicated that there was negligible population transfer to states $|F = 1, m_F = -1\rangle$ and $|F = 1, m_F = 1\rangle$ due to applied π-pulse of Raman beams. Thus our Raman beams dominantly excite the atomic transition

$$|F = 2, m_F = 0\rangle \rightarrow |F = 1, m_F = 0\rangle.$$

In the CAG setup, various events from MOT loading to detection of interference fringes are controlled by an in-house developed controller — Supervisory Control and Data Acquisition (SCADA) system. This controller system controls the sequence and duration of operation of various instruments such as accousto-optic modulators (AOMs), EOMs, power supplies, etc., in a synchronised manner. The controller system can provide more than 50 control signals to control instrument used in the experiments. The control signals are used in a series of steps to perform a sequence of different events such as formation of MOT, launching of atoms, implementation of Raman pulses for atom interferometry, detection of atoms in a particular state, etc. For each event, a number of instruments are used to execute various tasks. The duration and temporal resolution of the control signals are important for synchronization between different instruments used. Therefore, these control signals need to be generated with a temporal resolution of the order of few microseconds. Such a precise timing is difficult to achieve with processors. In order to meet this requirement, we have used a Field Programmable Gate Array (FPGA) based controller to generate the control signals and perform various tasks in the CAG setup. In order to achieve the temporal resolution of 1 μs, a 40 MHz reference clock is used for synchronization of events. The time synchronization between control signals is ~ 1 μs. To obtain precise control, the driving analog signals for AOMs and magnetic coil power supplies have 16-bit resolution.

A software framework is designed for performing the experiment which gives flexibility to generate control signals as per requirement. This framework ensures that the FPGA is re-configured to generate every desired pattern of the control signals. A software for

personal computer (PC) is also developed which provides an intuitive Graphical User Interface (GUI) for configuring the experimental parameters. There are 32 analog control signals (out of which 4 are isolated) to control AOMs, power supplies, etc. There are 24 digital signals to control various devices such as CCD camera, power supplies, shutters, etc. The CAG controller system is developed on NI make programmable automation controller c-RIO 9035.

For various measurements (such as fringe generation and Allan deviation) related to measurement of g, the CAG setup is operated with the repetition of the measurement cycle for a large number (several hundreds) of cycles. This process is manually difficult and time consuming. Therefore, an automation for the g-measurement is also implemented. For this purpose, data acquisition of atom interferometer signal from digital oscilloscope (Keysight DSOX 2024A) is done for different values of the chirp rate. A computational algorithm is implemented in software to compute the value of g from the acquired data set. The GUI finally displays the computed value of g.

4. RESULTS AND DISCUSSION

Among the forward-going and retro-reflected Raman beams, the Raman beam R_1 at frequency ω_1 with propagation in downward direction and the Raman beam R_2 at frequency ω_2 with propagation in upward direction are used in atom interferometry in our setup. After launching the cold atom cloud in the vertical upward direction and applying Raman pulses in the sequence $\pi/2 - T - \pi - T - \pi/2$, the population in $|F = 2\rangle$ state was measured to record the atom interferometer output. The total power in both Raman beams (R_1 and R_2) for these measurements was ~ 16 mW, with a power distribution in a ratio of 3:1. The duration of $\pi-$pulse was ~ 10 μs at this power and detuning. During the Raman pulses sequence, the frequency of one Raman beam R_1 was chirped at a chirp rate α before measurement of the output of atom interferometer. The interferometer output was measured for different values of chirp rate (α) and T. The results of these measurements, in which the population in $|F = 2\rangle$ state oscillates with the chirp rate (α), are shown in Fig. 4. These oscillations are known as interference fringes.

In Fig. 4 c, the plot shows the results of measurement of interference fringes with an increased resolution of 6.9 Hz/s in the chirp rate. This resolution of 6.9 Hz/s in chirp rate corresponds to 270 μGal reso-
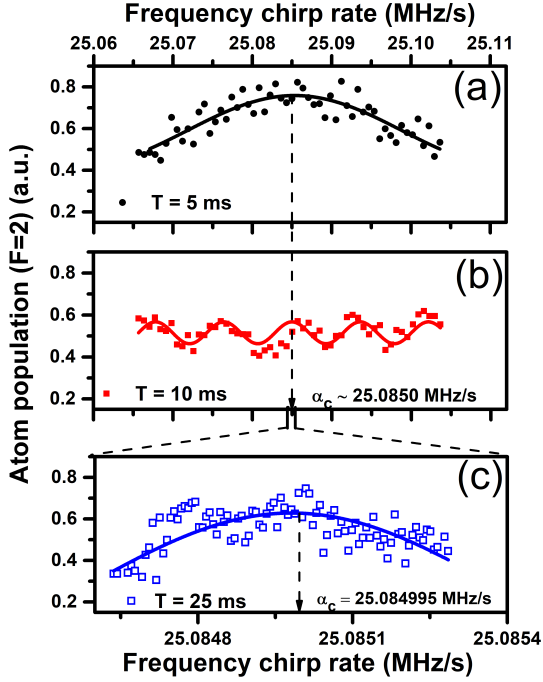
Fig. 4. The experimentally measured atom interferometry fringes showing variation in the atomic population with the Raman beam frequency chirp rate (α). Plots *a* and *b* show the fringes at the same scale of chirp rate for $T = 5$ ms (circles) and $T = 10$ ms (squares) respectively. The plot (*c*) shows the fringe for $T = 25$ ms (hollow squares) with chirp rate scale expanded nearby α_c. In plot c, the minimum step in frequency chirp rate was 6.9 Hz/s which corresponds to a step of $270\,\mu$Gal in terms of acceleration

lution in terms of acceleration g. Figure 4 shows the interferometric fringes taken without seismic vibration correction [46] for different values of T (5 ms (10 ms and 25 ms). The common peak in the fringes for all values of T gives the central chirp rate α_c for which net interferometric phase is zero. Using this value of the chirp rate, $\alpha_c = 25.084995$ MHz/s, we obtain the local value of g in our laboratory to be $g = 9.786173$ m/s^2. This value is in agreement with the value of g for Indore city calculated using Earth's Gravitational Model 2008 [47].

In order to estimate the sensitivity of our measurements, we have estimated the Allan deviation in the measurement of g. The Allan deviation, which is square root of Allan variance, is a commonly used parameter to characterize the temporal noise sensitivity in the precision measurements. For this, data of measured g value was recorded over a large number ($N = 600$) of cycles of interferometric measurement, at a fixed value of α and $T = 25$ ms. Each cycle of measurement in our
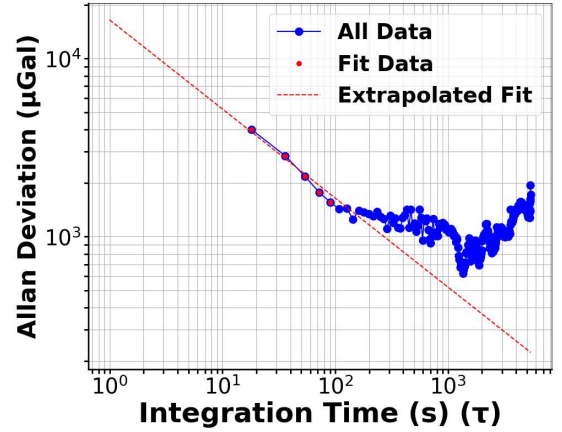
Fig. 5. Measured Allan deviation in g for the Raman pulses separation $T = 25$ ms

experiments takes nearly 18 seconds. From these measurements, the Allan variance, was calculated using the relation,

$$\sigma^2(\tau) = \frac{1}{2(M-1)} \sum_{i}^{M-1} \left(g_{i+1}(\tau) - g_i(\tau)\right)^2, \quad (6)$$

where M is the number of data points $g_i(\tau)$ each recorded at integration time of τ. The results of Allan deviation measurements are shown in Fig. 5 for different values of integration time (τ). Here, the dashed line shows a fit to the measured Allan deviation at smaller τ, corresponding to white noise dominated behavior of Allan deviation ($\sigma \propto \tau^{-1/2}$). From the graph in Fig. 5, it is obvious that the measured Allan deviation initially reduces with τ and reaches to minimum value of $621\,\mu$Gal at integration time $\tau = 1350$ s. With further increase in τ, the Allan deviation increases, which could be attributed to other noises in the setup such as drift and random walk. In future, various noises will be reduced to further enhance the sensitivity of the CAG setup.

5. CONCLUSION

We have developed a cold atom gravimeter (CAG) setup using a single laser system. In this device, the laser cooled ^{87}Rb atoms are launched in the vertical upward direction, like in a fountain. The gravitational acceleration of the Earth, g, acting on the atoms, has been measured by employing the velocity sensitive two-photon Raman pulse atom interferometry. The local value of g has been estimated with a sensitivity of $621\,\mu$Gal at the integration time of 1350 s.

REFERENCES

1. M. Inguscio and L. Fallani, *Atomic Physics: Precise Measurements and Ultracold Matter* (2013).

2. S. R. Mishra, S. P. Ram, S. K. Tiwari, and H. S. Rawat, *Dependence of in-situ Bose Condensate Size on Final Frequency of RF-Field in Evaporative Cooling*, Pramana **88**, 1 (2017).

3. I. Bloch, J. Dalibard, and S. Nascimbène, *Quantum Simulations with Ultracold Quantum Gases*, Nature Physics **8**, 267 (2012).

4. P. Asenbaum, C. Overstreet, M. Kim, J. Curti, and M. A. Kasevich, *Atom-Interferometric Test of the Equivalence Principle at the 10^{-12} Level*, Phys. Rev. Lett. **125** (191101 (2020).

5. P. Cladé, E. de Mirandes, M. Cadoret, S. Guellati-Khélifa, C. Schwob, F. Nez, L. Julien, and F. M. C. Biraben, *Determination of the Fine Structure Constant Based on Bloch Oscillations of Ultracold Atoms in a Vertical Optical Lattice*, Phys. Rev. Lett. **96**, 033001 (2006).

6. G. Rosi, F. Sorrentino, L. Cacciapuoti, M. Prevedelli, and G. Tino, *Precision Measurement of the Newtonian Gravitational Constant Using Cold Atoms,* Nature **510**, 518 (2014).

7. G. M. Tino and F. Vetrano, *Is It Possible to Detect Gravitational Waves with Atom Interferometers?* Class. Quant. Grav. **24**, 2167 (2007).

8. P. Delva and E. Rasel, *Matter Wave Interferometry and Gravitational Waves*, J. Mod. Opt. **56**, 1999 (2009).

9. P. Arora, A. Awasthi, V. Bharath, A. Acharya, S. Yadav, A. Agarwal, and A. S. Gupta, *Atomic Clocks: A Brief History and Current Status of Research in India*, Pramana **82**, 173 (2014).

10. A. Peters, K. Y. Chung, and S. Chu, *Measurement of Gravitational Acceleration by Dropping Atoms*, Nature **400**, 849 (1999).

11. I. Kulikov, *Gravitational Field Measurement with an Equilibrium Ensemble of Cold Atoms*, J. Mod. Opt. **53**, 1061 (2006).

12. J.-Y. Zhang, W.-J. Xu, S.-D. Sun, Y.-B. Shu, Q. Luo, Y. Cheng, Z.-K. Hu, and M.-K. Zhou, *A Car-Based Portable Atom Gravimeter and Its Application in Field Gravity Survey*, AIP Advances **11** (2021).

13. M. Wright, L. Anastassiou, C. Mishra, J. Davies, A. Phillips, S. Maskell, and J. Ralph, *Cold Atom Inertial Sensors for Navigation Applications*, Frontiers in Phys. **10**, 994459 (2022).

14. C.-Y. Li, J.-B. Long, M.-Q. Huang, B. Chen, Y.-M. Yang, X. Jiang, C.-F. Xiang, Z.-L. Ma, D.-Q. He, L.-K. Chen, and S. Chen, *Continuous Gravity Measurement with a Portable Atom Gravimeter*, Phys. Rev. A **108**, 032811 (2022).

15. C. Ruan, W. Zhuang, J. Yao, Y. Zhao, Z. Ma, C. Yi, Q. Tian, S. Wu, F. Fang, and Y. Wen, *A Transportable Atomic Gravimeter with Constraint-Structured Active Vibration Isolation*, Sensors **24** (2024).

16. L. Zhang, W. Gao, Q. Li, R.-B. Li, Z. Yao, and S. Lu, *A Novel Monitoring Navigation Method for Cold Atom Interference Gyroscope*, Sensors **19**, 222 (2019).

17. A. Hansen, Y.-J. Chen, J. Kitching, and E. Donley, *Point-Source Atom Interferometer Gyroscope*, Proc. Int. School of Physics «Enrico Fermi», Varenna, IT (2021).

18. F. Zhou, F. Jia, X. Liu, Y. Yu, J. Mei, J. Zhang, F. Xie, and Z. Zhong, *Improving the Spectral Resolution and Measurement Range of Quantum Microwave Electrometry by Cold Rydberg Atoms*, J. Phys. B **56**, 025501 (2022).

19. D. Braje, S. DeSavage, C. Adler, J. Davis, and F. Narducci, *A Frequency Selective Atom Interferometer Magnetometer*, J. Mod. Opt. **61**, 61 (2014).

20. J. Davis and F. Narducci, *A Proposal for a Gradient Magnetometer Atom Interferometer*, J. Mod. Opt. **55**, 3173 (2008).

21. M. Weitz, *Towards Controlling Larger Quantum Systems: From Laser Cooling to Quantum Computing*, IEEE J. Quant. Electron. **36**, 1346 (2000).

22. N. Poli, F.-Y. Wang, M. G. Tarallo, A. Alberti, M. Prevedelli, and G. M. Tino, *Precision Measurement of Gravity with Cold Atoms in an Optical Lattice and Comparison with a Classical Gravimeter*, Phys. Rev. Lett. **106**, 038501 (2011).

23. Y. Bidel, N. Zahzam, A. Bresson, C. Blanchard, A. Bonnin, J. Bernard, M. Cadoret, T. E. Jensen,

R. Forsberg, C. Salaun, S. Lucas, M. F. Lequentrec-Lalancette, D. Rouxel, G. Gabalda, L. Seoane, D. T. Vu, S. Bruinsma, and S. Bonvalot, *Airborne Absolute Gravimetry with a Quantum Sensor, Comparison with Classical Technologies*, J. Geophys. Research: Solid Earth **128**, e2022JB025921 (2022).

24. M. Kasevich and S. Chu, *Atomic Interferometry Using Stimulated Raman Transitions*, Phys. Rev. Lett. **67**, 181 (1991).

25. M. Kasevich and S. Chu, *Measurement of the Gravitational Acceleration of an Atom with a Light-Pulse Atom Interferometer*, Appl. Phys. B **54**, 321 (1992).

26. A. Peters, K. Y. Chung, and S. Chu, *High-Precision Gravity Measurements Using Atom Interferometry*, Metrologia **38**, 25 (2001).

27. G. Rosi, *Precision Gravity Measurements with Atom Interferometry*, PhD Thesis, University of Pisa (2012).

28. L. Zhou, Z.-Y. Xiong, W. Yang, B. Tang, W.-C. Peng, Y.-B. Wang, P. Xu, J. Wang, and M.-S. Zhan, *Measurement of Local Gravity via a Cold Atom Interferometer*, Chinese Phys. Lett. **28**, 013701 (2011).

29. S. Lellouch, K. Bongs, and M. Holynski, *Using Atom Interferometry to Measure Gravity*, Contemporary Phys. **63**, 138 (2022).

30. C.-F. Huang, A. Li, F.-J. Qin, J. Fang, and X. Chen, *An Atomic Gravimeter Dynamic Measurement Method Based on Kalman Filter*, Measurement Science and Technology **34**, 015013 (2022).

31. M. de Angelis, A. Bertoldi, L. Cacciapuoti, A. Giorgini, G. Lamporesi, M. Prevedelli, G. Saccorotti, F. Sorrentino, and G. M. Tino, *Precision Gravimetry with Atomic Sensors*, Measurement Science and Technology **20**, 022001 (2008).

32. A. E. Afanasiev, P. I. Skakunenko, and V. I. Balykin, *Cold Atom Gravimeter Based on an Atomic Fountain and a Microwave Transition*, JETP Lett. **119**, 84 (2024).

33. M. Gilowski, C. Schubert, T. Wendrich, P. Berg, G. Tackmann, W. Ertmer, and E. M. Rasel, *High Resolution Rotation Sensor Based on Cold Rubidium Atoms*, in *2009 IEEE Intern. Frequency Control Symposium Joint with the 22nd European Frequency and Time Forum*, 1173 (2009).

34. X. Wu, Z. Pagel, B. S. Malek, T. H. Nguyen, F. Zi, D. S. Scheirer, and H. Müller, *Gravity Surveys Using a Mobile Atom Interferometer*, Science Advances **5**, eaax0800 (2019).

35. B. Wu, Z. Wang, B. Cheng, Q. Wang, A. Xu, and Q. Lin, *The Investigation of a μgal-Level Cold Atom Gravimeter for Field Applications*, Metrologia **51**, 452 (2014).

36. T. Niebauer, *Gravimetric Methods-Absolute Gravimeter: Instruments Concepts and Implementation*, Geodesy **3**, 43 (2007).

37. N. Yu, J. Kohel, J. Kellogg, and L. Maleki, *Development of an Atom-Interferometer Gravity Gradiometer for Gravity Measurement From Space*, Appl. Phys. B **84**, 647 (2006).

38. G. M. Tino, F. Sorrentino, D. Aguilera, B. Battelier, A. Bertoldi, Q. Bodart, K. Bongs, P. Bouyer, C. Braxmaier, L. Cacciapuoti et al., *Precision Gravity Tests with Atom Interferometry in Space*, Nuclear Phys. B Proc. Suppl. **243**, 203 (2013).

39. A. Peters, K. Y. Chung, and S. Chu, *High-Precision Gravity Measurements Using Atom Interferometry*, Metrologia **38**, 25 (2001).

40. Z.-K. Hu, B.-L. Sun, X.-C. Duan, M.-K. Zhou, L.-L. Chen, S. Zhan, Q.-Z. Zhang, and J. Luo, *Demonstration of an Ultrahigh-Sensitivity Atom-Interferometry Absolute Gravimeter*, Phys. Rev. A **88**, 043610 (2013).

41. S. Singh, B. Jain, S. P. Ram, V. B. Tiwari, and S. R. Mishra, *A Single Laser-Operated Magneto-Optical Trap for Rb Atomic Fountain*, Pramana **95**, 1 (2021).

42. K. Moler, D. S. Weiss, M. Kasevich, and S. Chu, *Theoretical Analysis of Velocity-Selective Raman Transitions*, Phys. Rev. A **45**, 342 (1992).

43. J. N. Tinsley, *Construction of a Rubidium Fountain Atomic Interferometer for Gravity Gradiometry*, PhD Thesis, University of Liverpool (2019).

44. M. Kasevich and S. Chu, *Measurement of the Gravitational Acceleration of an Atom with a Light-Pulse Atom Interferometer*, Appl. Phys. B **54**, 321 (1992).

45. A. J. Dunning, *Coherent Atomic Manipulation and Cooling: Interferometric Laser Cooling and Composite Pulses for Atom Interferometry*, Springer Int. Publ. (2015).

46. M. Guo, J. Bai, D. Hu, Z. Tang, J. You, R. Chen, and Y. Wang, *A Vibration Correction System for Cold Atom Gravimeter*, Measurement Science and Technology **35**, 035011 (2023).

47. N. K. Pavlis, S. A. Holmes, S. C. Kenyon, and J. K. Factor, T*He Development and Evaluation of the Earth Gravitational Model 2008*, J. Geophys. Research: Solid Earth **117** (2012).